Talanta 81 (2010) 37–43

Contents lists available at ScienceDirect

Talanta

journal homepage: www.elsevier.com/locate/talanta

Highly sensitive and fast responding CO sensor based on Co_3O_4 nanorods

Dewyani Patil[a], Pradip Patil[a,*], Vijayanand Subramanian[b], Pattayil A. Joy[b], Hari S. Potdar[b,**]

[a] Department of Physics, North Maharashtra University, Jalgaon 425 001, Maharashtra, India
[b] Physical and Materials Chemistry Division, National Chemical Laboratory, Dr. Homi Bhabha Road, Pune 411 008, Maharashtra, India

ARTICLE INFO

Article history:
Received 19 August 2009
Received in revised form 9 November 2009
Accepted 10 November 2009
Available online 18 November 2009

Keywords:
Co_3O_4 nanorods
CO sensor
Semiconductor gas sensors
HRTEM
XPS
XRD

ABSTRACT

Co_3O_4 nanorods (diameters ~6–8 nm and lengths ~20–30 nm) were synthesized for the first time through a simple co-precipitation/digestion method by calcination of cobalt hydroxyl carbonate in air and their CO gas sensing properties were investigated. The Co_3O_4 nanorods exhibited outstanding gas sensing characteristics such as, higher gas response (~6.55–50 ppm CO gas at 250 °C), extremely rapid response (~3–4 s), fast recovery (~5–6 s), excellent repeatability, good selectivity and lower operating temperature (~250 °C). Furthermore, the Co_3O_4 nanorods are able to detect up to 5 ppm for CO with reasonable sensitivity (~3.32) at an operating temperature 250 °C and they can be reliably used to monitor the concentration of CO over the range (5–50 ppm). The experimental results clearly demonstrate the potential of using the Co_3O_4 nanorods as sensing material in the fabrication of CO sensors. Plausible CO sensing mechanism of the Co_3O_4 nanorods is also discussed.

1. Introduction

Carbon monoxide (CO) is one of the most harmful pollutants, which presents significant health risks [1–3] and studies have shown that it interacts with the haemoglobin and damages the human body by producing a reduction in cellular respiration [4]. This has stimulated considerable interest for scientific research to develop simple and cost-effective chemical sensors for the detection of CO in recent years and many efforts, in this field, are today devoted to the synthesis of novel sensing materials with enhanced performance [1,4–7]. Up till now, the metal oxide semiconductors have been widely investigated in the past decades as gas sensing materials because of their low cost and power consumption, simplicity of fabrication and use, versatility in detecting a wide range of toxic/flammable gases, and stability in harsh environments [8,9]. The metal oxide semiconductors such as SnO_2 [4], In_2O_3 [5] and ZnO [10] have been investigated as CO sensing materials.

Recent studies reveal that the nanostructured metal oxides with reduced dimensionality (i.e. in the form of nanoparticles, nanorods, nanotubes, nanowires and nanoribbons) have ultrahigh sensitivity to different gases due to their small grain size and large surface-to-volume ratio [11–16]. Various nanostructured metal oxide materials like CdO nanoparticles [11], α-Fe_2O_3 nanorods [12], SnO_2 nanotubes [13], In_2O_3 nanowires [14], CuO nanoribbons [15] and ZnO nanorods [16] have been evaluated as gas sensing materials during the past few years.

Cobalt oxide (Co_3O_4), an important magnetic p-type semiconductor, has received considerable attention in the past few years due to its application potential in many technological areas such heterogeneous catalysis, anode material in lithium rechargeable batteries, sensors, electrochromic devices, solar energy absorber, etc. [17–19]. Consequently, different methods for synthesizing the Co_3O_4 nanostructures with various morphologies have been reported [20–22]. For example, Dong et al. [20] prepared the Co_3O_4 nanowires having the diameters of ~20–100 nm and physical lengths of about 10–20 μm by directly heating pure cobalt foils in air. Lakshami et al. [21] synthesized the Co_3O_4 nanofibers using the sol gel method combined with a template synthesis technique. Nam et al. [22] demonstrated the feasibility of employing the viruses to synthesize and assemble the Co_3O_4 nanowires as an electrode material for lithium ion batteries. Although, different methods for synthesizing the nanostructured Co_3O_4 in the form of nanowires and nanofibers were reported, there are only few reports on the gas sensing properties of nanostructured Co_3O_4 [23,24]. A two-step polyol process to synthesize nanostructured Co_3O_4 with different morphologies such as nanoplates, well-organised cabbage like structures and microspherical composites was reported recently by Cao et al. [23]. These authors investigated the CO and alcohol sensing properties of the synthesized nanostructured Co_3O_4. The synthesized nanostructured Co_3O_4 exhibited good sensitivity (>8–50 ppm), response and recovery times (<10 s), remarkable selectivity and high stability to alcohol at an operating temperature

* Corresponding author at: Department of Physics, North Maharashtra University, Post Box 80, Jalgaon 425 001, Maharashtra, India. Tel.: +91 2572257474.
** Corresponding author. Tel.: +91 2025902476.
E-mail addresses: pnmu@yahoo.co.in (P. Patil), hs.potdar@ncl.res.in (H.S. Potdar).

0039-9140/$ – see front matter © 2009 Elsevier B.V. All rights reserved.
doi:10.1016/j.talanta.2009.11.034

of 300 °C. However, it was found to be insensitive to 50 ppm CO at 300 °C and the resistance change was still at a much lower level for 1000 ppm CO. Li et al. [24] prepared the Co_3O_4 nanotubes by a thermal decomposition of $Co(NO_3)_2{\cdot}6H_2O$ within an ordered porous alumina templates and investigated the gas sensing characteristics of these nanotubes exposed to H_2 and alcohol. The prepared Co_3O_4 nanotubes exhibited an excellent sensitivity to hydrogen and alcohol at room temperature.

Herein, we report for the first time a successful synthesis of Co_3O_4 nanorods by using a simple and low cost co-precipitation/digestion route without any template or a capping agent. Sensing characteristics of the Co_3O_4 nanorods to CO gas were systematically investigated.

2. Experimental

The nanostructured Co_3O_4 was synthesized by a simple co-precipitation/digestion method. In this method, equal volumes of aqueous solutions of $Co(NO_3)_2{\cdot}6H_2O$ (0.0339 M) and K_2CO_3 (0.0627 M) were added drop-wise to 200 ml of double distilled water kept at 70 °C with continuous stirring, under argon atmosphere to achieve precipitation of cobalt hydroxyl carbonate. The necessary pH value between 7 and 8 required for supersaturation was instantly reached by this process. The precipitation obtained after completion of addition was digested in mother liquor at the same temperature for duration of 8 h. The cobalt hydroxyl carbonate precursor obtained were thoroughly washed with distilled water several times to avoid K^+ ion contamination and further dried in an oven at 70 °C. The as-dried sample is named as D-8 corresponding to 8 h digestion time. The thermogravimetric analysis (TGA) showed that the hydroxyl carbonate decomposes to give the corresponding oxide at 250 °C. The composition of the hydorxyl carbonate was found to be $Co(OH)(CO_3)_{0.5}{\cdot}0.11H_2O$ as revealed from TGA and CH analysis. Hence, a part of the as-dried sample was calcined in air at 300 °C for 5 h to obtain the powder of nanostructured cobalt oxide. The calcined sample is named as C-8 corresponding to 8 h digestion.

The structure of the calcined sample C-8 was investigated by using X-ray diffraction (XRD) technique. The X-ray diffraction patterns were recorded with a Rigaku diffractometer (Miniflex Model, Rigaku, Japan) having Cu Kα (λ = 0.1542 nm). The high resolution transmission electron microscopy (HRTEM) was used to determine the particle size and the morphology of the nano-sized powder with JEOL 1200 EX. The X-ray photoelectron spectroscopy (XPS) analysis was carried out using a V.G. Microtech Scientific spectrometer, ESCA 3000, U.K. equipped with two ultrahigh vacuum chambers. The pressure in the chambers during the experiments was about 10^{-9} Pa. The XPS spectra were recorded with un-monochromatized Mg Kα radiation (photon energy = 1253.6 eV) at a constant 50 eV pass energy. The core level binding energies were corrected with the C 1s binding energy of 284.9 eV.

The nanostructured Co_3O_4 powder was pressed into pellets under a pressure of 15 MPa and the ohmic contacts were made with the help of silver paste to form the sensing element. The gas sensing studies were carried out on these sensing elements in a static gas chamber to sense CO in air ambient. The sensing element was kept directly on a heater in the gas chamber and the temperature was varied from 50 to 400 °C. The temperature of the sensing element was monitored by chromel–alumel thermocouple placed in contact with the sensor. The known volume of the CO was introduced into the gas chamber pre-filled with air and it was maintained at atmospheric pressure. The electrical resistance of the sensing element was measured before and after exposure to CO using a sensitive digital multi-meter (METRAVI 603). The performance of the sensing element is presented in terms of gas response (S), which is defined as:

$$S = \frac{R_{gas}}{R_{air}} \quad (1)$$

where R_{air} and R_{gas} are the electrical resistance values of the sensor element in air and in the presence of CO gas, respectively.

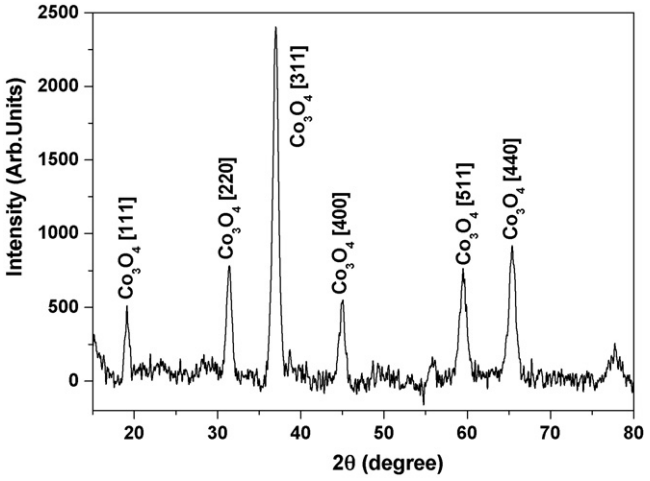

Fig. 1. XRD pattern of nanostructured Co_3O_4 prepared with 8 h digestion time.

3. Results and discussion

3.1. XRD results

Fig. 1 shows the XRD pattern of the calcined sample C-8. It exhibits the diffraction peaks at 2θ values of 19.08°, 31.36°, 36.97°, 45.02°, 59.42° and 65.37°, which are attributed to the formation of spinel oxide Co_3O_4 with cubic lattice parameter of a = 8.083 Å. This is in good agreement with the reported value for Co_3O_4 powder (a = 8.084 Å; JCPDS #9-418). The crystallite size was estimated by using the Scherrer formula:

$$t = \frac{k\lambda}{B\cos\theta} \quad (2)$$

where t is the average size of the crystallite, assuming that the grains are spherical, k is 0.9, λ is the wavelength of X-ray radiation, B is the peak full width at half maximum (FWHM) and θ is the angle of diffraction. The crystalline size of the calcined sample C-8 is found to be in the range of 10–20 nm.

3.2. Surface morphology

The HRTEM images of the calcined sample C-8 are shown in Fig. 2. As can be seen from Fig. 2(a), mostly the Co_3O_4 particles are in the form of rods (diameter = 6–8 nm, length = 20–30 nm) with presence of few spherical crystallite particles of size ~2–3 nm in the calcined sample C-8. The parallel lattice fringes across almost all the primary particles are clearly visible (Fig. 2(b)) which confirms the perfectly oriented aggregation of the nanoparticles of Co_3O_4. It is clearly seen that the aggregated Co_3O_4 rod like particles are composed of many small Co_3O_4 nanoparticles. In order to confirm further the formation of the nanorods, we have calculated the surface area of both the rods and spherical particles by taking the dimensions from the HRTEM images. The calculated surface area of the nanorods is around 100 m^2/g and the surface area of the spherical particle is around 187 m^2/g. However, the observed surface area is 95 m^2/g. If we consider only the presence of spherical particles the surface area value would have been nearly equal to 187 m^2/g. Thus, the experimentally observed surface area value

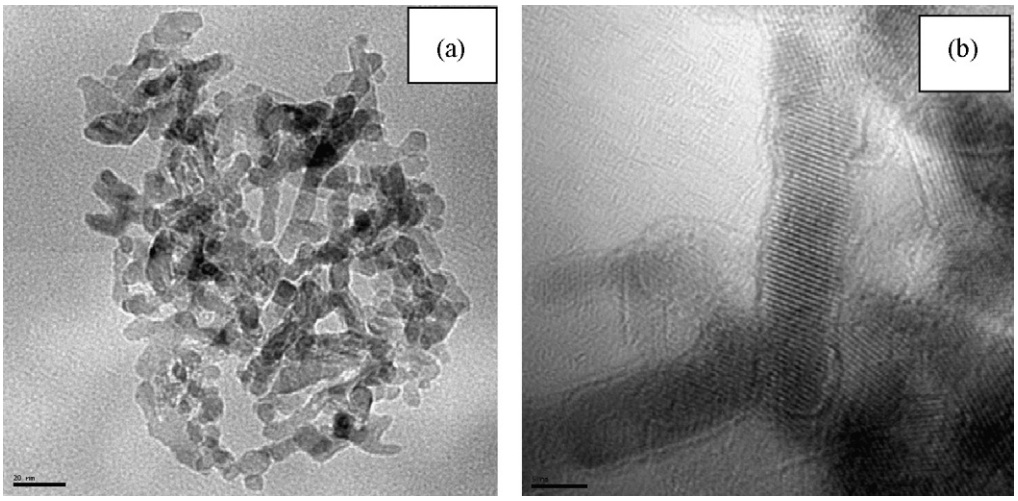

Fig. 2. HRTEM images of (a) nanorod aggregates of Co_3O_4 and (b) primary nanoparticles of Co_3O_4.

i.e. 95 m^2/g is much lower than the calculated surface area value of 187 m^2/g, which reveals the presence of more rod shaped particles in our sample.

3.3. XPS results

In order to further confirm the formation of Co_3O_4 nanorods, the calcined sample C-8 was also analyzed by the XPS. Fig. 3(a) shows the deconvoluted Co 2p spectrum of the calcined sample C-8. It exhibits two major peaks with binding energy values of 779.95 and 795.18 eV, corresponding to Co $2p_{3/2}$ and Co $2p_{1/2}$ doublet core level peaks, respectively, of the Co_3O_4 phase [25,26]. The Co $2p_{3/2}$–Co $2p_{1/2}$ peak separation is approximately 15.23 eV. These binding energy values are comparable to that reported for Co_3O_4 indicating the presence of Co^{2+} and Co^{3+} species in the calcined sample C-8. The formation of Co_3O_4 is further confirmed by the presence of weak satellite peak between the main peaks Co $2p_{3/2}$ and Co $2p_{1/2}$ [27,28]. The typical satellite peak is observed at a binding energy value of 789.2 eV, about 9.02 eV higher than 779.95 eV, where the peak of Co $2p_{3/2}$ appears.

The O 1s spectrum of the calcined sample C-8 (Fig. 3(b)) is deconvoluted into two peaks at 529.94 and 531.94 eV [20,29,30]. The lower binding energy peak at 529.94 eV corresponds to oxygen species in the spinel Co_3O_4 phase [29]. The peak at 531.94 eV indicates the presence of –OH (hydroxyl) species adsorbed on the surface of the sample [20,30]. Thus, from the XRD, XPS and TEM measurements, it is clear that the calcined sample C-8 is composed of aggregated Co_3O_4 rod like particles composed of many small Co_3O_4 nanoparticles.

3.4. Formation mechanism of Co_3O_4 nanorods

When potassium carbonate and cobalt nitrate solutions are dropped from separate burette to distilled water at 70 °C, the following chemical reaction occurred to precipitate cobalt hydroxyl carbonate precursor at pH ~7.5–8.0. The XRD study confirmed the formation of polycrystalline cobalt hydroxyl carbonate with composition shown by equation:

$$Co^{2+} + OH^- + 0.5CO_3{}^{2-} + 0.5H_2O \rightarrow Co(OH)(CO_3)_{0.5}\cdot 0.11H_2O \downarrow + 0.39H_2O \quad (3)$$

The probable mechanism of formation of rod shaped morphology in the cobalt hydroxyl carbonate precursor and resulting Co_3O_4 spinel type oxide is described as given below: initially, the cobalt hydroxy carbonate particles are nucleated which grow with the increase in digestion time when are in contact with solution having pH ~7.5–8.5 by Oswald ripening process. These precursor particles have all the crystal faces well developed. It is reported that the energy of different faces is not the same. Therefore, the high energy faces come together to minimize their energy and get connected by oriental attachment mechanism to form rods. The same morphological features are preserved during the calcination process and hence rod shaped spinel type of Co_3O_4 oxide could be obtained.

3.5. CO gas sensing characteristics

The CO gas sensing experiments were performed at different temperatures in order to find out the optimum operating temperature for CO gas detection. Before exposing to the CO gas, the sensing element was allowed to equilibrate inside the gas chamber at an operating temperature for 1 h. A number of experiments have been carried out to measure the gas response as a function of the operating temperature. All the time the gas response of the sensor element has approximately constant values, indicating the repeatability of the sensor. The effect of an operating temperature on the gas response to 50 ppm CO gas of the synthesized Co_3O_4 nanorods is shown in Fig. 4(a). The relationship between the gas response and the operating temperature exhibits a trend of "increase-maximum-decay" behavior to 50 ppm CO gas. At low temperatures, the gas response is relatively low (e.g. 1.66 at 100 °C), but it increases rapidly with an increase in the operating temperature. At 250 °C, the gas response is peaked to its maximum value of 6.55. Above 250 °C, the gas response decreased as the operating temperature increased further. Thus, the optimum operating temperature for the Co_3O_4 nanorods to detect CO gas was at 250 °C, which is the modest from the viewpoint of semiconducting oxide gas sensors. Hence, to investigate the CO gas sensing properties such as response and recovery characteristics, reproducibility and selectivity, 250 °C was chosen as the operating temperature.

When the commercially available Co_3O_4 powder was used, the gas response to 50 ppm of CO gas (Fig. 4(b)) remains fairly constant at ~2.20 between the operating temperatures 200–300 °C. It can also be seen that the gas response of the Co_3O_4 nanorods is about three times greater than that of commercial Co_3O_4 powder, indicating the improved sensivity of the Co_3O_4 nanorods. These observations reveal that the CO sensing ability of Co_3O_4 is significantly enhanced when it is in the form of nanorods. The enhanced CO gas sensing performance of Co_3O_4 nanorods over that of commercially available Co_3O_4 powder may be attributed to their

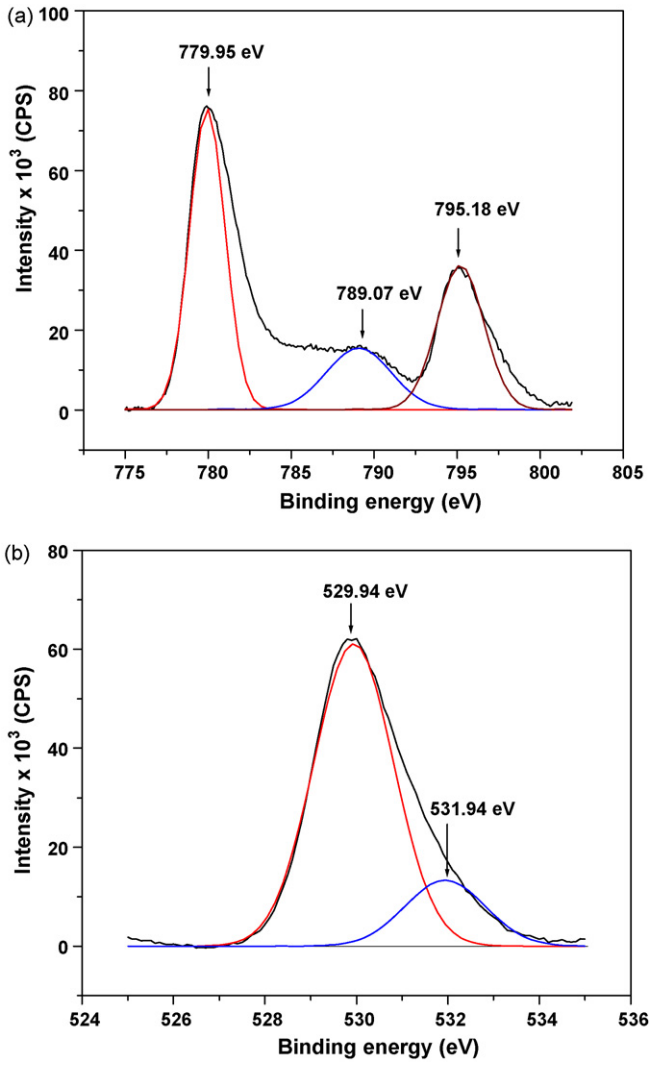

Fig. 3. XPS spectra (a) Co 2p and (b) O 1s of nanostructured Co_3O_4 prepared with 8 h digestion time.

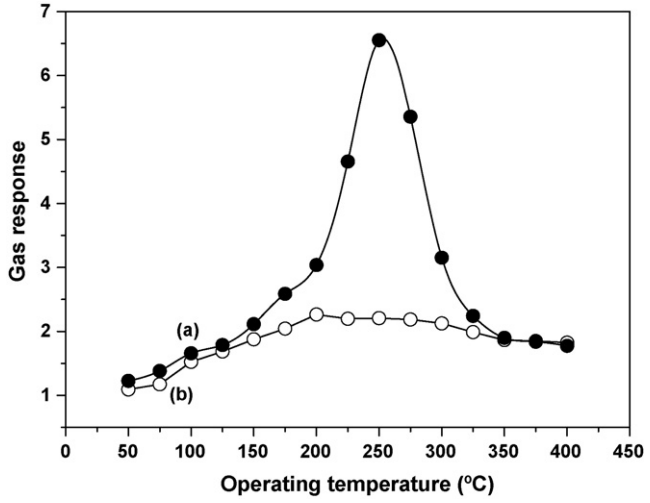

Fig. 4. Effect of operating temperature on the gas response of (a) Co_3O_4 nanorods and (b) commercially available Co_3O_4 powder to 50 ppm CO gas.

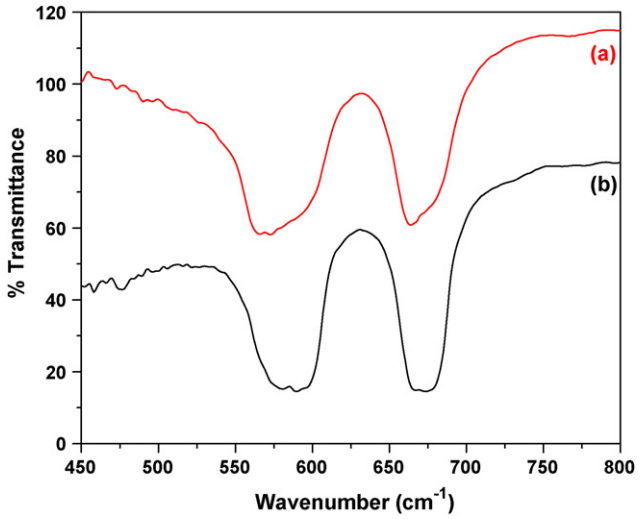

Fig. 5. FTIR spectra of (a) Co_3O_4 nanorods and (b) commercially available Co_3O_4 powder.

smaller size and higher specific surface area of the rod morphology. Generally, gas sensor response of metal oxide semiconductors increases with decrease in their size due to higher surface area and defect density [31]. Therefore, it is expected that the Co_3O_4 nonorods will have more defects/active sites at the surface, which is confirmed by performing the FTIR studies on both the samples. The FTIR spectra of Co_3O_4 nanorods and commercially available Co_3O_4 powder are shown in Fig. 5(a) and (b), respectively. The FTIR spectrum of the Co_3O_4 nanorods (Fig. 5(a)) exhibits the presence of two distinctive bands at 568 and 664 cm^{-1} originating from the stretching vibration of the metal oxygen bond, which confirms the formation of the Co_3O_4 spinel oxide. The first band is due to the Co^{3+} in an octahedral position while the second one corresponds to the Co^{2+} in tetrahedral position. Since in the nanostructured materials, these two bands slightly shift to lower wave numbers as compared to the bulk counter part due to large number of defects at the surface [32,33]. Thus, the FTIR spectroscopy result confirms the presence of more defect/active sites at the surface of the Co_3O_4 nanorods.

The response and recovery characteristics are important for evaluating the performance of gas sensors. The response and recovery times are defined as the time required for the sensor-resistance to change by 90% of the final resistance. The response and recovery characteristics of the Co_3O_4 nanorods to 50 ppm CO gas at an operating temperature 250 °C is shown in Fig. 6. Five samples were tested from each batch and each sample was tested three times. It was observed that the resistance of the sensing element increases when exposed to the CO gas. As can be seen from Fig. 6, the sensor responds very rapidly after introduction of CO gas and recovers immediately when it is exposed to air. The Co_3O_4 nanorods have response time of ~3–4 s and the recovery time of ~5–6 s. This behavior can be attributed to the higher surface-to-volume ratio of the nanorods and stronger bonding between nanoparticles.

The reproducibility and stability are important parameters to be considered when evaluating the performance of a sensor. It is useful to have both a stable base line resistance and a reproducible signal change to a given analyte concentration. The reproducibility and stability of the Co_3O_4 nanorods were measured by repeating the test four times. The gas response of the Co_3O_4 nanorods upon periodic exposure to 50 ppm CO gas at an operating temperature of 250 °C is shown in Fig. 7. The Co_3O_4 nanorods show good reproducibility and reversibility upon repeated exposure and removal of CO under same conditions. Thus, the Co_3O_4 nanorods exhibit good stability as well as an excellent repeatability of the response. This

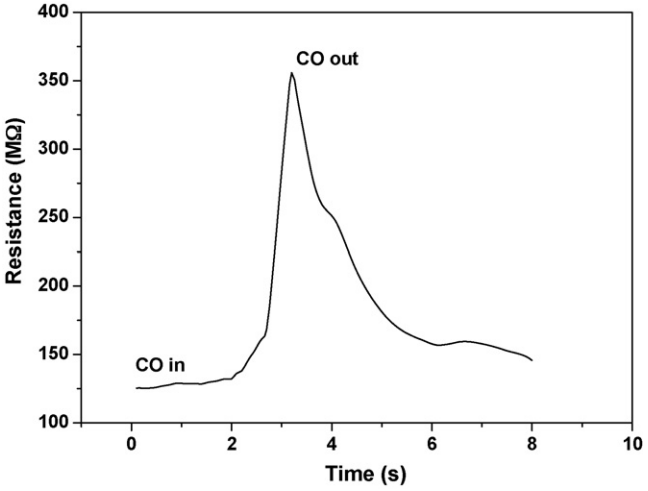

Fig. 6. Response of Co_3O_4 nanorods to 50 ppm CO gas at an operating temperature of 250 °C.

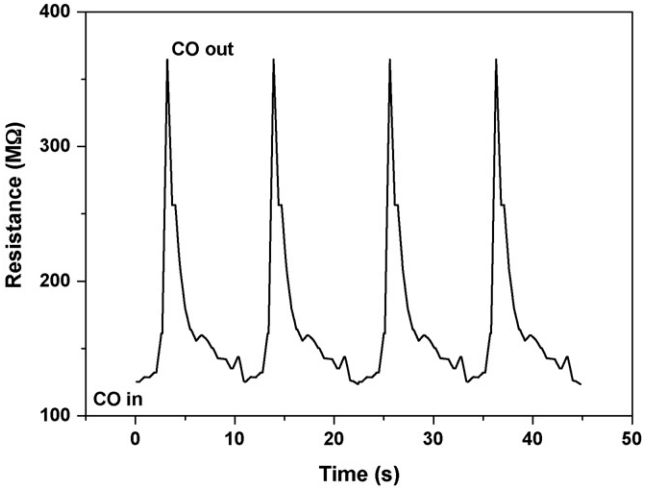

Fig. 7. Repetitive response of Co_3O_4 nanorods to 50 ppm CO gas at an operating temperature of 250 °C.

suggests that the Co_3O_4 nanorods can be used as a reusable sensing material for the detection of CO gas.

The dependence of the gas response of the synthesized Co_3O_4 nanorods on the CO gas concentration at an operating temperature of 250 °C is shown in Fig. 8. It was observed that the gas response increases linearly up to 50 ppm CO gas and thereafter it saturates. It is found that the response of Co_3O_4 nanorods can be empirically represented as $y = 2.91 + 0.0718x$, $R^2 = 0.9990$, where x, y and R^2 represents the CO concentration, gas response and correlation coefficient, respectively. The broken curve shows the linear fit to the experimental data, illustrating clearly good quality of the fit. The linear relationship between the gas response and the CO gas concentration at low concentrations (5–50 ppm) may be attributed to the availability of sufficient number of sensing sites to act upon the CO gas. The low gas concentration implies a lower surface coverage of gas molecules, resulting into lower surface interaction between the surface of the nanorods and the gas molecules. The increase in the gas concentration increases the surface reaction due to a large surface coverage. Further increase in the surface interaction will be gradual when saturation of the surface coverage of gas molecules is reached. Thus, the maximum gas response was obtained at an operating temperature of 250 °C for the exposure of 50 ppm of CO gas. The Co_3O_4 nanorods are able to detect up to 5 ppm for CO gas

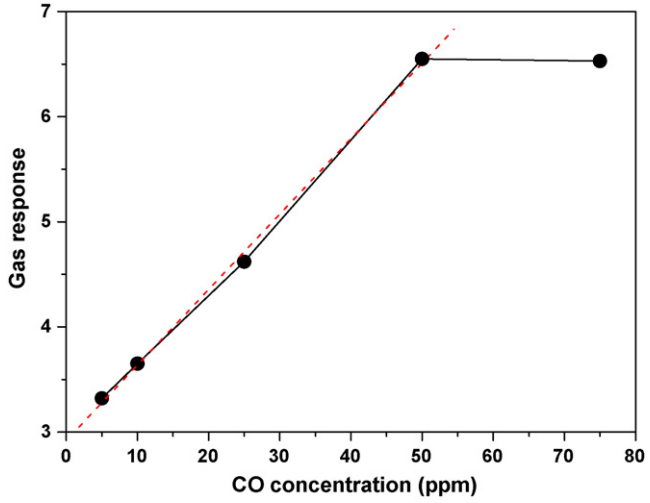

Fig. 8. Relationship between gas response of Co_3O_4 nanorods and CO gas concentration.

with good response (~3.32) at an operating temperature 250 °C. The linearity of the gas response in the low CO gas concentration range (5–50 ppm) suggests that the Co_3O_4 nanorods can be reliably used to monitor the concentration of CO gas over this range.

Selectivity is an important parameter of gas sensors and it is the ability of a sensor to respond to a certain gas in presence of other gases. Theoretically, the sensors should have high response to some gases and little or no response to other gases in the same surroundings. To study the selective behavior of the Co_3O_4 nanorods to CO at an operating temperature of 250 °C, the gas response towards H_2, liquid petroleum gas (LPG), CO_2 and ethanol with concentration 50 ppm each were also measured. The corresponding results are shown in Fig. 9. The Co_3O_4 nanorods exhibit higher response to CO (6.55), whereas it shows a considerably lower response (<3.51) to H_2, LPG, CO_2 and ethanol. The selectivity coefficient (K) of CO to another gas is defined as [34]:

$$K = \frac{S_{CO}}{S_B} \quad (4)$$

where S_{CO} and S_B are the responses of sensors in CO and B gas, respectively. The selectivity coefficients for the Co_3O_4 nanorods were 2.22 to H_2, 2.64 to CO_2, 1.86 to LPG and 2.28 to ethanol.

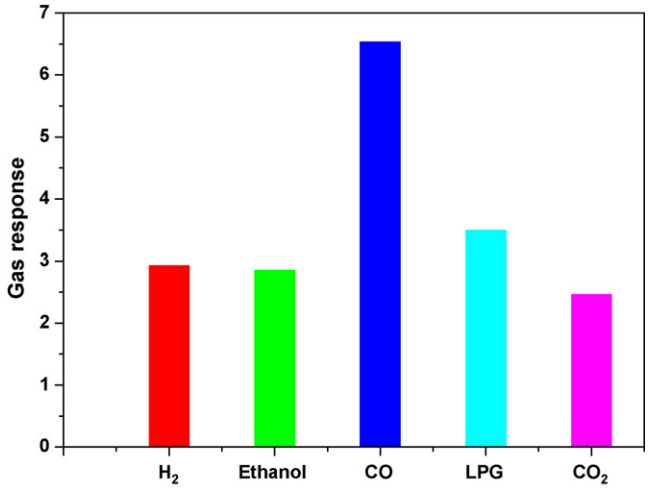

Fig. 9. Bar chart showing the gas response of Co_3O_4 nanorods for different gases. The gas concentration and operating temperature in all cases were 50 ppm and 250 °C, respectively.

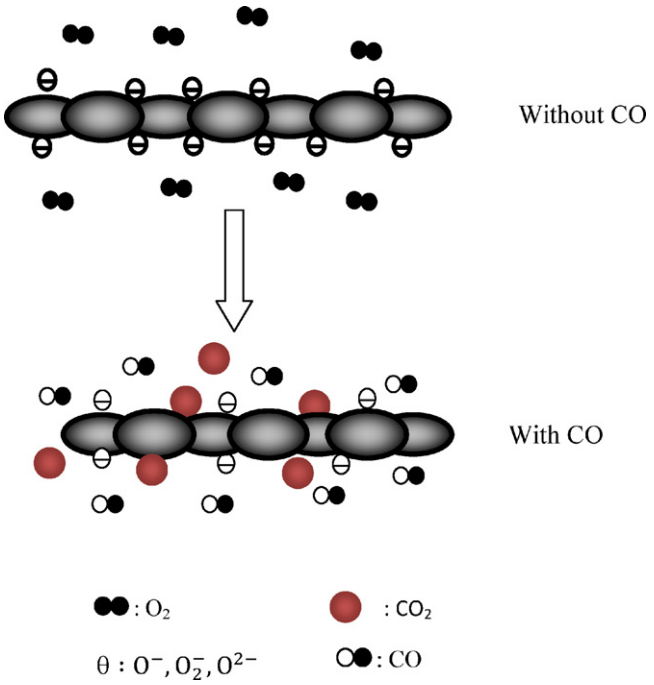

Fig. 10. Schematic diagram of CO sensing process of the Co_3O_4 nanorod.

The selectivity coefficients for the Co_3O_4 nanorods were 2.22 to H_2, 2.64 to CO_2, 1.86 to LPG and 2.28 to ethanol. Commonly, the selectivity coefficient of sensors should be more than 5 [35]. Thus, it was found that the Co_3O_4 nanorods synthesized by using a chemical co-precipitation method/digestion method by calcination of cobalt hydroxyl carbonate precursor in air could not reach the criterion. The experimental results indicate that the Co_3O_4 nanorods based sensor has a reasonably good selectivity to CO. Based on the observed results, it can be concluded that the formation of Co_3O_4 nanorods is effective not only in enhancing the relative response factor but also in making it selective for the detection of CO.

Taking into account the results of gas sensing experiments, it is concluded that the Co_3O_4 nanorods have good CO sensing properties such as higher gas response, good selectivity, short response time, fast recovery, excellent repeatability and lower operating temperature.

3.6. CO gas sensing mechanism

Here, we suggest a possible mechanism to explain qualitatively the observed CO sensing properties of Co_3O_4 nanorods. The sensing performance of semiconductor oxides is usually attributed to the adsorption and desorption of oxygen on the surface of the oxides. It is important to note that the trend in the changing resistance of the p-type of semiconductor sensor with the concentration of the reducing gas was completely opposite to that of an n-type of sensor [8,9,36]. The Co_3O_4 is a p-type oxide semiconductor and thus, its majority carriers are holes. The CO sensing process is based on the changes in the resistance of the Co_3O_4 which is controlled by the CO species and the amount of the chemisorbed oxygen on the surface [37,38].

By only considering a single Co_3O_4 nanorod, the sensing process of CO gas is schematically depicted in Fig. 10. It is known that a certain amount of oxygen from air is adsorbed on the surface of the Co_3O_4. The adsorbed oxygen molecules capture free electrons from the nanorods and become oxygen anion species such as O_2^- or O^-. The reaction kinematics may be explained by the following reactions [39,40]:

$$\begin{aligned} &O_2(\text{gas}) + e^- \rightarrow O_2^-(\text{ads}) \\ &O_2^-(\text{ads}) + e^- \rightarrow 2O^-(\text{ads}) \\ &2O^-(\text{ads}) + e^- \rightarrow O_2^-(\text{ads}) \end{aligned} \quad (5)$$

In these processes, there exists a transition temperature (~180 °C) below which oxygen adsorbed on the surface is mainly in the form of O_2^-, where as above which chemisorbed oxygen dominates in the form of O^- and O^{2-} [41]. For Co_3O_4, the oxygen adsorption produces an increase in the hole density in the valence band, which increases their conductivity. The electron transfer from the conduction band to the chemisorbed oxygen results into an increase in the hole density. As a consequence, an increase in the conductivity of the Co_3O_4 is observed.

When the Co_3O_4 is exposed to reducing gas like CO, the reaction between CO and adsorbed oxygen (O_2^- or O^-) proceeds by Langmuir–Hinshelwood mechanism [42]:

$$\begin{aligned} &CO_{gas} \rightarrow CO_{ads} \\ &CO_{ads} + O^- \rightarrow CO_2 + e^- \end{aligned} \quad (6)$$

This reaction decreases of the hole density in the surface charge layer and increases the resistance of the Co_3O_4 nanorods.

4. Conclusions

We have successfully synthesized the Co_3O_4 nanorods at low cost by using a chemical co-precipitation/digestion method by calcination of cobalt hydroxyl carbonate precursor in air. TEM study revealed the formation of nanorods having the diameters and lengths of ~6–8 nm and about 20–30 nm, respectively. The gas response to 50 ppm of CO gas is maximum at an operating temperature 250 °C and it is found to be ~6.55. The response time was nearly 3–4 s and the recovery time was found to be 5–6 s. The synthesized Co_3O_4 nanorods are able to detect up to 5 ppm for CO with reasonable response at an operating temperature 250 °C. Further, it was shown that the Co_3O_4 nanorods can be reliably used to monitor the concentration of CO gas over the range (5–50 ppm). These results indicate that the Co_3O_4 nanorods are indeed very attractive CO gas sensing materials.

Acknowledgement

One of us (PP) gratefully acknowledges the financial support from University Grants Commission (UGC), New Delhi, India through the major research project no. F 34-3/2008 (SR).

References

[1] N. Wu, M. Zhao, J.G. Zheng, C. Jiang, B. Myers, S. Li, M. Chyu, S.X. Mao, Nanotechnology 16 (2005) 2878–2881.
[2] A. Srivastava, R.K. Jain, Mater. Chem. Phys. 105 (2007) 385–390.
[3] W.J. Moon, J.H. Yu, G.M. Choi, Sens. Actuators B: Chem. 87 (2002) 464–470.
[4] T. Zhang, L. Liu, Q. Qi, S. Li, G. Lu, Sens. Actuators B: Chem. 139 (2009) 287–291.
[5] K.I. Choi, H.R. Kim, J.H. Lee, Sens. Actuators B: Chem. 138 (2009) 497–503.
[6] B. Bahrami, A. Khodadadi, M. Kazemeini, Y. Mortazavi, Sens. Actuators B: Chem. 133 (2008) 352–356.
[7] L. Zhang, J. Hu, P. Song, H. Qin, K. An, X. Wang, M. Jiang, Sens. Actuators B: Chem. 119 (2006) 315–318.
[8] C.C. Wang, S.A. Akbar, M.J. Madou, J. Electroceram. 2 (1998) 273–282.
[9] N. Barsan, U. Weimar, J. Electroceram. 7 (2001) 143–167.
[10] J.X. Wang, X.W. Sun, H. Huang, Y.C. Lee, O.K. Tan, M.B. Yu, G.Q. Lo, D.L. Kwong, Appl. Phys. A 88 (2007) 611–615.
[11] R.B. Waghulade, R. Pasricha, P.P. Patil, Talanta 72 (2007) 594–599.
[12] C. Wu, P. Yin, X. Zhu, C.O. Yang, Y. Xie, J. Phys. Chem. B 110 (2006) 17806–17812.
[13] Y. Jia, L. He, Z. Guo, X. Chen, F. Meng, T. Luo, M. Li, J. Liu, J. Phys. Chem. C 113 (2009) 9581–9587.
[14] C. Li, D. Zhang, B. Lei, S. Han, X. Liu, C. Zhou, J. Phys. Chem. B 107 (2003) 12451–12455.
[15] X. Gou, G. Wang, J. Yang, J. Park, D. Wexler, J. Mater. Chem. 18 (2008) 965–969.
[16] C.C. Li, Z.F. Du, L.M. Li, H.C. Yu, Q. Wan, T.H. Wang, Appl. Phys. Lett. 91 (2007) 032101.

[17] L.F. Liotta, G.D. Carlo, G. Pantaleo, G. Deganello, Catal. Commun. 6 (2005) 329–336.
[18] H.J. Nam, T. Sasaki, N. Koshizaki, J. Phys. Chem. B 110 (2006) 23081–23084.
[19] L. Fu, Z. Liu, Y. Liu, B. Han, P. Hu, L. Cao, D. Zhu, Adv. Mater. 17 (2005) 217–221.
[20] Z. Dong, Y. Fu, Q. Han, Y. Xu, H. Zhang, J. Phys. Chem. C 111 (2007) 18475–18478.
[21] B.B. Lakshami, C.J. Patrissi, C.R. Martin, Chem. Mater. 9 (1997) 2544–2550.
[22] K.T. Nam, D.W. Kim, P.J. Yoo, C.Y. Chiang, N. Meethong, P.T. Hammond, Y.M. Chiang, A.M. Belcher, Science 312 (2006) 885–888.
[23] A.M. Cao, J.S. Hu, H.P. Liang, W.G. Song, L.J. Wan, X.L. He, X.G. Gao, S.H. Xia, J. Phys. Chem. B 110 (2006) 15858–15863.
[24] W.Y. Li, L.N. Xu, J. Chen, Adv. Funct. Mater. 15 (2005) 851–857.
[25] C.V. Chenck, J.G. Dillard, J.W. Murray, J. Colloid Interf. Sci. 95 (1983) 398–409.
[26] M. Oku, Y. Sato, Appl. Surf. Sci. 55 (1992) 37–41.
[27] T.J. Chuang, C.R. Brundle, D.W. Rice, Surf. Sci. 59 (1976) 413–429.
[28] M.A. Langell, M.D. Anderson, G.A. Carson, L. Peng, S. Smith, Phys. Rev. B 59 (1999) 4791–4798.
[29] L. Armelao, D. Barreca, S. Gross, E. Tondello, Surf. Sci. Spectra 8 (2001) 14–23.
[30] B. Varghese, T.C. Hoong, Z. Yanwu, M.V. Reddy, B.V.R. Chowdari, A.T. Wee, T.B.C. Vincent, C.T. Lim, C.H. Sow, Adv. Funct. Mater. 17 (2007) 1932–1939.
[31] X.J. Huang, Y.K. Choi, Sens. Actuators B: Chem. 122 (2007) 659–671.
[32] C.B. Wang, C.W. Tang, S. Gau, S.H. Chien, Catal. Lett. 101 (2005) 59–63.
[33] Y.Z. Wang, Y.X. Zhao, C.G. Gao, D.S. Liu, Catal. Lett. 116 (2007) 136–142.
[34] M. Siemons, U. Simon, Sens. Actuators B: Chem. 126 (2007) 595–603.
[35] X. Loua, S. Liu, D. Shi, W. Chua, Mater. Chem. Phys. 105 (2007) 67–70.
[36] Z. Liu, T. Yamazaki, Y. Shen, T. Kikuta, Appl. Phys. Lett. 90 (2007) 173119.
[37] H. Huang, O.K. Tan, Y.C. Lee, T.D. Tran, M.S. Tse, X. Yao, Appl. Phys. Lett. 87 (2005) 163123.
[38] A. Ponzoni, E. Comini, G. Sberveglieri, J. Zhou, S.Z. Deng, N.S. Xu, Y. Ding, Z.L. Wang, Appl. Phys. Lett. 88 (2006) 203101.
[39] H. Mbarek, M. Saadoun, B. Bessis, Mater. Sci. Eng. C 26 (2006) 500–504.
[40] K. Arshak, I. Gaidan, Sens. Actuators B: Chem. 111 (2005) 58–62.
[41] D. Kohl, Sens. Actuators 18 (1989) 71–113.
[42] D. Koziej, K. Thomas, N. Barsan, F. Thibault-Starzyk, U. Weimar, Catal. Today 126 (2007) 211–218.